NONDESTRUCTIVE TESTING AND EVALUATION
2020, VOL. 35, NO. 3, 252–265
https://doi.org/10.1080/10589759.2020.1774580

Taylor & Francis
Taylor & Francis Group

Check for updates

A low-cost geometry calibration procedure for a modular cone-beam X-ray CT system

V. Nguyen[a], J. De Beenhouwer[a], J. G. Sanctorum[b], S. Van Wassenbergh[c], S. Bazrafkan[a], J. J. J. Dirckx[b] and J. Sijbers[a]

[a]Imec - Vision Lab, Department of Physics, University of Antwerp, Universiteitsplein 1, Antwerp, 2610, Belgium; [b]Biophysics and BioMedical Physics (BIMEF) Lab, University of Antwerp, Antwerp, Belgium; [c]Functional Morphology Lab, University of Antwerp, Antwerp, Belgium

ABSTRACT

Accurate knowledge of the acquisition geometry of a CT scanning system is key for high quality tomographic imaging. Unfortunately, in modular X-ray CT setups, geometry misalignment occurs each time the setup is changed, which calls for an efficient calibration procedure to correct for geometric inaccuracies. Although many studies have been dealing with the calibration of X-ray CT systems, these are often specifically designed for one setup and/or expensive.

In this work, we explore the possibilities of a low-cost, easy-to-build, and modular phantom, constructed from LEGO bricks, which serves as a structure to hold small metal beads, for geometric calibration of a tomographic X-ray system. By estimating the bead coordinates using deep learning, and minimizing center-to-center distances of the metal beads between measured and reference projection data, geometry parameters are derived. With simulated as well as real experiments, it is shown that the LEGO phantom can be used to accurately estimate the geometry of a modular X-ray CT system.

ARTICLE HISTORY
Received 14 January 2020
Accepted 6 May 2020

KEYWORDS
LEGO phantom; geometry calibration; cone-beam CT; deep learning

1. Introduction

X-ray Computed Tomography (CT) involves the recording of a set of two-dimensional (2D) X-ray images (radiographs) of an object, followed by a digital three-dimensional (3D) reconstruction. To obtain high quality tomographic images, the position of the X-ray source with respect to the object, as well as the position and orientation of the detector need to be accurately known. If the geometry of the X-ray system is undefined or uncertain, the resulting reconstructed image will suffer from misalignment artifacts and blurring. Hence, the X-ray scanning system needs to be calibrated by estimating the geometric relationship between the X-ray source and the detector with respect to the rotation axis prior to image reconstruction.

Literature on the calibration of X-ray acquisition systems can be subdivided into two main categories: self-calibration methods [1–4], which calculate the geometry parameters of the acquisition system directly from the acquired radiographs of the target objects, and techniques that rely on a calibration phantom [5–9].

CONTACT V. Nguyen van.nguyen@uantwerpen.be
© 2020 Informa UK Limited, trading as Taylor & Francis Group

In the work of Parkinson et al. [1], 2D rigid misalignment is estimated based on geometric characteristics of the object projections. The orientation of the rotation axis is determined as the angle between the axial axis of the cylinder holding the object, and the vertical axis of the 2D projection image. In another study, Kingston et al. [2] estimated four geometry parameters by iteratively refining the sharpness of reconstructed images. Both methods are, however, computationally expensive. Moreover, 2D transformations can only partially correct for 3D geometrical misalignment, because the out-of-plane transformations are not taken into account.

Other self-calibration techniques have been presented to estimate out-of-plane misalignments. For example, Kyungtaek et al. [3] used the projection trajectory of a fixed point to estimate the translation and vertical tilt of the rotation axis, which can only be applied to a parallel 3D geometry. Wang et al. [4] introduced a two step algorithm to consecutively correct the misalignments caused by vertical translation and tilt, followed by horizontal translation correction. In general, self-calibration is object dependent and therefore requires calibration prior to each scan, even without a change of the geometry setup. Moreover, these methods usually focus on a specific type of misalignment (e.g. only in-plane rotations of the detector). Cone beam X-ray CT systems whose sources, detectors, and rotation stages are highly modular usually require a representation of the geometry in higher degrees of freedom. An extensive calibration method is therefore needed to calibrate such types of cone beam X-ray CT systems.

Another class of calibration methods rely on fiducial markers to estimate the geometry parameters. Most phantom-based X-ray CT calibration methods employ specifically designed phantoms in which the position of the markers is measured accurately using Coordinate Measuring Machines (CMM). For example, Liu et al. [5] introduced a phantom that carried 12 spherical zirconia markers placed on a triple helix glass structure. Another well designed phantom presented by Cho et al. and Chetley et al. [6,7] contained two circular rings of evenly placed steel balls on an acrylic cylinder.

Efforts have been made to reduce the calibration phantom complexity. For example, Gross et al. [9] built a phantom with vertically arranged beads and proposed an algebraic model to recover the geometry parameters. It was assumed that the system describes a perfect circular rotation, in which case the bead's projection follows an elliptical trajectory on the detector plane. Mennessier et al. [8] presented a comprehensive analytical method to estimate geometry parameters for a cone beam geometry using a 14-marker phantom. The phantom was designed to handle all possible interference patterns between the markers on the projection images.

Specialized calibration phantoms that are used in the phantom based calibration methods usually come with a high cost and are often dedicated to a specific setup. A low-cost, fast, and flexible calibration procedure that can be easily adapted to various cone beam X-ray CT systems is therefore required. Attempts have been made to build them from LEGO bricks. The use of LEGO elements was first proposed to construct a mounting structure of an optical system [10], thereby exploiting the low tolerances (20 μm) on their design. Moreover, the variations in shapes and sizes of the LEGO bricks make them excellent components to build a calibration phantom that is optimized for the geometry of the X-ray CT system under concern. In a first effort, Levine et al. [11] built a LEGO calibration phantom for a CT system consisting of two LEGO spacers holding three spherical markers. The position of the spheres was measured with a CMM and the

phantom was used to detect systematic errors of a medical X-ray scanning system. However, it was not used to calibrate the system's geometry.

In this paper, we introduce a calibration method using a LEGO phantom containing metal beads, strategically placed in the bearing bricks. Since the LEGO bricks and metal beads come in different sizes, our phantom easily adapts to various X-ray CT systems. The paper is structured as follows. Section 2 presents our proposed methodology to build a calibration phantom using LEGO bricks and metal beads along with the process to extract the bead centers accurately with deep learning and to estimate the geometrical misalignments using least squares optimization. Section 3 discusses the simulation experiments that were performed to validate the feasibility of our proposed method, as well as the experiments and results using real LEGO phantom datasets. Finally, further discussion and conclusions are presented in Section 4.

2. Methodology

In what follows, we will describe a modular X-ray CT system, after which we introduce our geometry calibration procedure.

2.1. Acquisition system

Figure 1(a) shows the stereoscopic X-ray system that is used for the experimental measurements: the 3-Dimensional DYnamic MOrphology using X-rays (3D^{2}YMOX) system, dedicated to morphological and biomechanical research on animals [12]. The system consists of two orthogonal X-ray source detector pairs and a rotation stage which is mounted on a wheeled tripod. The sources are mounted on two ceiling gantries that allow them to be easily positioned in 3D space. The side handle bars attached to each source control its rotations around three principle axes. In addition, the two detectors are put on two trolleys with hydraulic lifts so as to flexibly adjust their horizontal and vertical position. Moreover, each detector has a steering wheel that manipulates its orientation in 3D space. Consequently, each device is positioned independently from the others. In any new installation, the position of the sources and stage as well as the position and orientation of the detector in the 3D^{2}YMOX system can change dramatically. With such a setup, it is challenging to align the sources, detectors and rotation stage properly

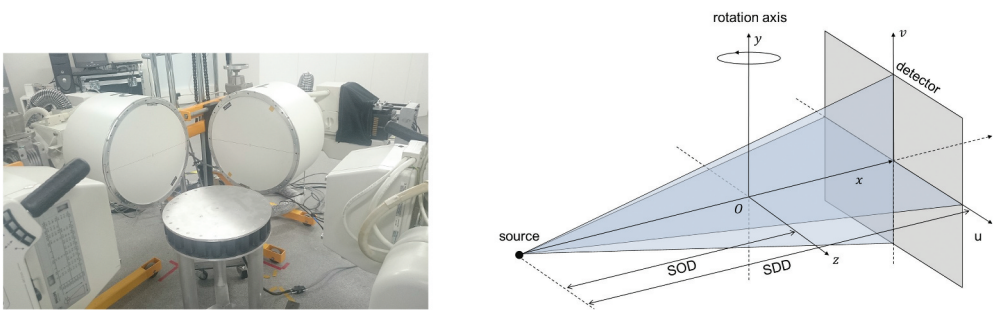

(a) (b)

Figure 1. 3D^{2}YMOX system (a) and visualization of a cone beam geometry without misalignments (b).

and to accurately measure the geometry. It is therefore essential to perform a calibration in order to estimate the system geometry as accurately as possible. Similar systems are used worldwide for biomechanical analysis, such as XROMM [13].

2.2. Geometry parameterization

A general cone beam geometry is shown in Figure 1(b). The source, the rotation axis, and the vertical axis through the detector center are all aligned within a single plane that is perpendicular to the detector surface. In this geometry, the source detector distance (SDD) and source object distance (SOD) refer to the shortest distances from the source to the detector and from the source to the rotation axis, respectively. In a highly modular system such as the 3D^{2}YMOX, misalignments are induced by manual arrangement of the sources, detectors, and rotation stage. Six parameters are used to model detector translation $\left\{\Delta x^d, \Delta y^d, \Delta z^d\right\}$ and detector orientation $\left\{\theta^d, \phi^d, \eta^d\right\}$ in 3D space.

In addition, six more parameters are used to define the object orientation $\{\theta^o, \phi^o, \eta^o\}$ and translation $\{\Delta x^o, \Delta y^o, \Delta z^o\}$ with respect to the rotation axis coordinate system *Oxyz*. The rotation axis coordinate system *Oxyz* is chosen as the reference with respect to which the rest of the system geometry is parameterized with 12 degrees of freedom ($\beta = \{\Delta x^o, \Delta y^o, \Delta z^o, \theta^o, \phi^o, \eta^o, \Delta x^d, \Delta y^d, \Delta z^d, \theta^d, \phi^d, \eta^d\}$). In our work, the SDD and SOD are assumed to be measured in advance. However, SOD deviation can also be included in the calibration procedure.

2.3. Geometry estimation

Calibration methods based on markers (metal beads) make use of the projections of the markers onto the detector to estimate the geometry parameters. The reference and corresponding measured coordinates of marker k in projection n on the detector plane are denoted as $(u_{nk}^{ref}, v_{nk}^{ref})$ and $(u_{nk}^{mea}, v_{nk}^{mea})$, respectively. For every projection angle, the vector that represents the system geometry is transformed accordingly in terms of the misalignment parameters. The reference $(u_{nk}^{ref}, v_{nk}^{ref})$ coordinates are then calculated as the intersections of the rays from the source through the bead centers (x_k, y_k, z_k) with the detector plane.

The measured $(u_{nk}^{mea}, v_{nk}^{mea})$ coordinates are extracted from the acquired projection data using deep learning (BeadNet, section 3.2). BeadNet is trained from the predefined neural network model Resnet-50 [14] using a simulated dataset containing X-ray bead projections from different geometry configurations. The simulated datasets are generated with a CAD (Computer Aided Design) projector [15]. Bead ROIs and their corresponding ground truth center coordinates are extracted from the simulated projection to build the BeadNet training dataset. The geometry parameter set β is estimated by iteratively minimizing the total Euclidean norm between the reference $(u_{nk}^{ref}, v_{nk}^{ref})$ and the measured $(u_{nk}^{mea}, v_{nk}^{mea})$ coordinates across all projections p_n $(n = 1, \ddot{A}\tilde{a}\acute{\epsilon}\tilde{I}, N)$ and marker centers $k = 1, \ddot{A}\tilde{a}\acute{\epsilon}\tilde{I}, K$ with the interior point algorithm [16]:

$$\hat{\beta} = \arg\min_{\beta}\left\{\sum_{n=1}^{N}\sum_{k=1}^{K}\left[\left(u_{nk}^{ref}(\beta) - u_{nk}^{mea}\right)^2 + \left(v_{nk}^{ref}(\beta) - v_{nk}^{mea}\right)^2\right]\right\} \tag{1}$$

where $\beta = \{\Delta x^o, \Delta y^o, \Delta z^o, \theta^o, \phi^o, \eta^o, \Delta x^d, \Delta y^d, \Delta z^d, \theta^d, \phi^d, \eta^d\}$.

2.4. LEGO phantom design strategy

To facilitate the extraction of markers from the measured X-ray projections, the phantom must be built so as to enhance the contrast between the LEGO structure and the metal beads in the radiographs. The LEGO structure is constructed from as few LEGO bricks as possible in order to easily extract the metal bead centers from the projections. The steel markers with a diameter of (4950 ± 10) μm are placed inside the hollow cylinders of the bricks, by pushing the LEGO bricks on a flat surface to press the metal beads exactly one diameter deep into the cylinders. These bead-bearing bricks are then placed strategically in the phantom so that no two beads are within the same vertical brick layer (colored in blue in Figure 2(a)). This design strategy avoids overlapping beads in the projections.

Moreover, the beads are placed such that their projection trajectories cover as much of the detector's field-of-view as possible. As studied by Ferrucci et al. [17], the further away the markers are from the rotation axis, the larger the coordinate changes due to geometry misalignments can be. A strategic design of the phantom helps to address these coordinate deviations in the misaligned geometry. Depending on the size of the target system's field-of-view, the phantom dimensions and the number of metal beads can be adjusted accordingly.

2.5. Data preprocessing

The acquired radiographs from the 3D^{2}YMOX system show geometrical distortions induced by the image intensifier [18]. In order to correct the projection data, an aluminum grid of circular holes, as described in [19], is first placed in front of the detector intensifier to acquire its X-ray image. Then, XMALab 1.5.1 [20] is used to compute the distortion correction map using the aluminum grid image. The undistortion matrix contains 2D coordinate interpolation coefficients that map the pixel values from

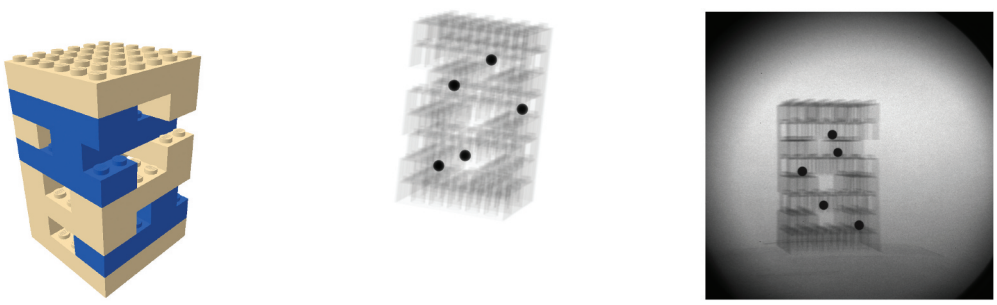

(a) (b) (c)

Figure 2. An example of a LEGO phantom (a), a simulated radiograph (b), and an X-ray radiograph acquired with the 3D^{2}YMOX system (c).

the original to the new coordinates, thereby removing the pincushion and sigmoidal distortion effect on the acquired projections.

3. Experiments and results

3.1. Generation of simulated datasets

The simulated datasets were generated using the phantom STL models and the ASTRA CAD projector toolbox [15]. Triangular meshes, representing the LEGO structure and the metal bead surfaces, were first constructed. The system vector geometry was calculated with respect to the misalignment parameters β for every projection angle with the ASTRA Toolbox [21,22]. The geometry parameters were uniformly sampled in the intervals shown in Table 1. Then, X-ray radiographs of the phantom were simulated using a certain energy spectrum (10 energy bins in a range from 50 keV to 150 keV) with the predefined geometries. The detector was a flat panel of 2048×2048 pixels with a pixel size of 142 μm, which corresponds to the detector model of the 3D^{2}YMOX system. Figure 2 shows an example of a LEGO phantom (Figure 2(a)), a simulated projection (Figure 2(b)), and a real radiograph acquired with the 3D^{2}YMOX system (Figure 2(c)).

To study the impact of the marker position errors on the geometry parameters estimation, we first tested whether the geometry parameters were calibrated correctly with the ground truth bead centers. Results (not shown) indeed showed that all geometry parameters were estimated close to the ground truth values with translation errors less than 0.1 μm and orientation errors of about 1 μdeg.

To simulate marker center extraction inaccuracies, random coordinate errors with mean of (150 ± 80) μm were added to the ground truth coordinates with which 50 deviated trajectory profiles were generated. The effect of these induced biases on the estimated geometry parameters are shown in Table 2. As seen in the table, the parameters $\left\{\Delta x^o, \Delta z^o, \Delta z^d, \theta^o, \phi^o, \eta^o, \theta^d, \phi^d\right\}$ are estimated with small errors of (13 ± 12) μm, (23 ± 16) μm, (10 ± 8) μm, (12 ± 9) mdeg, (23 ± 18) mdeg, (12 ± 10) mdeg, and (14 ± 7) mdeg on average, respectively, while the object and the detector translation errors $\left\{\Delta y^o, \Delta x^d, \Delta y^d\right\}$ are (174 ± 105) μm, (250 ± 210) μm, (291 ± 176) μm on average, respectively. The detector orientation parameters ϕ^d, η^d are also largely different from the ground truth values with (147 ± 92) mdeg and (182 ± 134) mdeg mean error, respectively.

3.2. Training BeadNet for center coordinate regression

BeadNet was trained using the predefined ResNet-50 model [14], which is a widely-used deep learning model for morphological studies. The training dataset was generated as to mimic all possible geometry configurations of the 3D^{2}YMOX system, for which 400 projections were simulated for each of the 120 angles covering 360° rotation. Each set corresponds to 400 randomly generated detector and object orientations and translations along with varied SODs. Afterwards, 25 bead ROIs were extracted from every projection along with their ground truth center coordinates. Two BeadNets were trained separately for each center coordinate. We evaluated the BeadNet accuracy compared to that of the conventional method [23] with 85 simulated datasets. As can be seen from Table 3, with

Table 1. Geometry parameter ranges for the simulation experiments.

Distances (mm)		Translation parameters (mm)						Orientation parameters (deg)					
SDD	SOD	Δx^o	Δy^o	Δz^o	Δx^d	Δy^d	Δz^d	θ^o	ϕ^o	η^o	θ^d	ϕ^d	η^d
1143	[680, 820]	[−27, 17]	[−35, 17]	[−31, 13]	[−20, 17]	[−25, 15]	[−31, 13]	[−9, 9]	[73, 219]	[−5, 5]	[−3, 5]	[−4, 4]	[−5, 4]

Table 2. Estimation of the geometry parameters with center extractions errors.

Estimated translation errors (μm)						Estimated orientation errors (mdeg)					
Δx^o	Δy^o	Δz^o	Δx^d	Δy^d	Δz^d	θ^o	ϕ^o	η^o	θ^d	ϕ^d	η^d
13 ± 12	174 ± 105	23 ± 16	250 ± 210	291 ± 176	10 ± 8	12 ± 9	23 ± 18	12 ± 10	14 ± 7	147 ± 92	182 ± 134

BeadNet, the marker centers (u, v) are estimated more accurately as the average errors are of (0.27 ± 0.16) pixel and (0.25 ± 0.15) pixel, while the estimation errors are (0.62 ± 0.49) pixel and (0.54 ± 0.36) pixel for the conventional method, respectively. The results show that BeadNet significantly improves the marker center estimation in terms of accuracy and precision compared to the conventional method.

3.2.1. Reconstruction from simulated phantom projections

In practice, multiple objects are usually scanned with the same geometry setup. That is, the sources and detectors are placed in a fixed position in terms of the detector translation $\{\Delta x^d, \Delta y^d, \Delta z^d\}$ and orientation $\left\{\theta^d, \phi^d, \eta^d\right\}$ in the acquisition while the target objects are altered to acquire different datasets. Hence, the phantom based calibration algorithm must be able to distinguish between the parameters of the detector and the object so that the estimated geometry can be used to reconstruct the other objects scanned with the same geometry. To mimic this process, we reconstructed a test phantom that was also built from LEGO bricks with the estimated geometry. With known shape and structure, this phantom is a reliable model to assess 3D CT quality and to evaluate the artifacts caused by geometry misalignments.

Figure 3 shows two cross-sections of the test phantom reconstructions before (Figure 3(a)) and after (Figure 3(b)) geometry correction. Severe misalignment artifacts are visible in the reconstructed slice before correcting the geometry (Figure 3(a)), while after alignment, the distinctive brick structure is clearly revealed in Figure 3(b). Figure 3(c) shows two intensity profiles (corresponding to the red lines in Figure 3(a) and Figure 3(b)) of the reconstructed slice before (blue) and after (orange) calibration, respectively. As the lines (red) cross the LEGO bricks (Figure 3(a,b)), more pronounced peaks can be observed after geometry alignment (orange) compared to before calibration (blue) (Figure 3(c)), showing that the reconstruction contrast is significantly improved.

Table 3. Bead center extraction errors.

	u (pixel)	v (pixel)
Conventional method	0.62 ± 0.49	0.54 ± 0.36
BeadNet	0.27 ± 0.16	0.25 ± 0.15

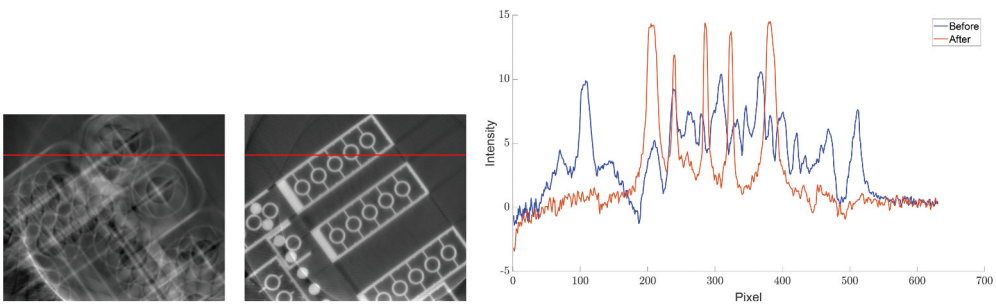

(a) before (b) after (c) intensity profile

Figure 3. Cross-sections of the reconstructed volumes from the simulated LEGO phantom dataset before (a) and after (b) geometry calibration. As shown in the intensity line profile (c), the peaks are more pronounced after the geometry alignment (orange) compared to before calibration (blue).

Moreover, the geometry was corrected with only the detector misalignments prior to the reconstruction, demonstrating that our calibration algorithm is able to distinguish the object from the detector misalignments.

3.2.2. Calibration of the 3D^{2}YMOX system using the LEGO phantom

A real LEGO phantom was used to calibrate the geometry of the 3D^{2}YMOX system, with which the phantom radiographs were acquired. The real datasets were firstly flatfield and log corrected before they were undistorted to remove the pincushion and sigmoidal distortion with the procedure described in Section 2.5. The bead center trajectories were extracted with BeadNet to estimate the geometry parameters. Initialization and calibrated geometry parameters are shown in Table 4. The SOD and SDD were measured after the acquisition using a laser meter. The other geometry parameters were initialized to zero.

3.2.3. Reconstruction from real phantom projections

In this experiment, we reconstructed two different object datasets acquired in the same geometrical system setup as with which the calibration dataset was scanned. The vector geometry was manipulated by the detector parameters before computing CT volumes. Figure 4 shows the reconstructed slices of the test phantom before (Figure 4(a)) and after (Figure 4(b)) calibration with their corresponding line profiles across the reconstructed LEGO brick (Figure 4(c)). The reconstructed volume before the geometry alignment suffered from severe artefacts in the form of smeared edges of the LEGO bricks.

In Figure 4(b), however, the shapes and edges of the bricks are better recovered in the reconstruction. Figure 4(c) shows two intensity profiles that are plotted across the LEGO brick before (blue) and after (orange) calibration, respectively. Before calibration, the LEGO bricks are blurry, as can be observed from the intensity peaks, which are dispersed throughout the line profile (blue plot in Figure 4(c)). After geometry correction, the brick structure is recovered with six peaks (orange plot in Figure 4(c)) corresponding to the intersections of the line (red) and the LEGO brick edges (Figure 4b).

3.2.4. Reconstruction of a real piglet

A piglet dataset was used for reconstruction to evaluate the accuracy of the estimated geometry. Figure 5(a) shows a CT slice extracted from the piglet reconstructed volume with uncalibrated geometry. As can be seen from the figure, the internal structure of the piglet is severely distorted by the geometry misalignment. The geometry was corrected with the estimated detector parameters before computing the CT volume from the piglet dataset. After calibration, the artifacts are reduced and the piglet skeleton is clearly recovered in the reconstructed slices shown in Figure 5(b) (for example, the spine at the lower right of the images). Figure 5(c) shows a better contrast between the bone and the soft tissues as the peak is more pronounced in the line profile after geometry alignment (orange) compared to before correction (blue).

4. Discussion & conclusions

In this paper, we presented a simple, yet effective method to construct and use a LEGO phantom to calibrate the 3D^{2}YMOX system, which is a highly modular X-ray CT system.

Table 4. Calibration of the geometry parameters for the 3D^{2}MOX system.

	Distances (mm)			Translation parameters (mm)						Orientation parameters (°)				
	SDD	SOD	Δx^o	Δy^o	Δz^o	Δx^d	Δy^d	Δz^d	θ^o	ϕ^o	η^o	θ^d	ϕ^d	η^d
Initialization	1100	270	0	0	0	0	0	0	0	0	0	0	0	0
Estimation	1100	270	− 23.19	25.65	− 9.10	10.69	− 22.34	− 2.91	0.18	111.70	0.64	− 0.13	1.09	1.10

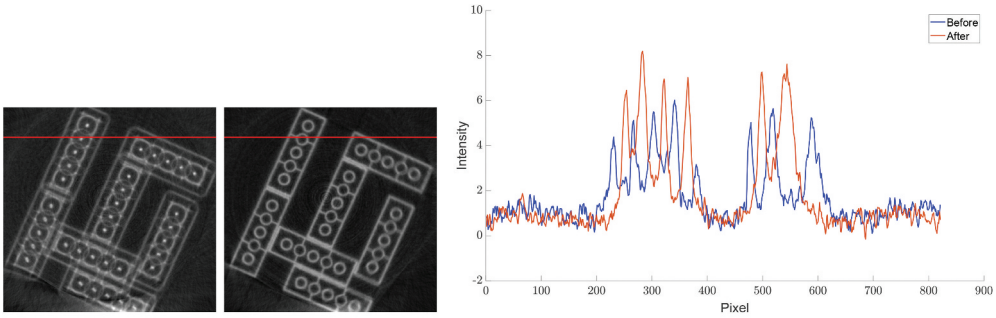

(a) before (b) after (c) intensity profile

Figure 4. Cross-sections from the reconstructions of a LEGO test phantom before (a) and after (b) geometry calibration. Without compensating the geometry misalignment, the internal brick structures are distorted (a). In (b), the artifacts are significantly reduced revealing sharp edges and shapes of the LEGO bricks. The intensity profile (c) also shows better contrast in the reconstructed slice after geometry correction (orange) compared to before (blue) calibration.

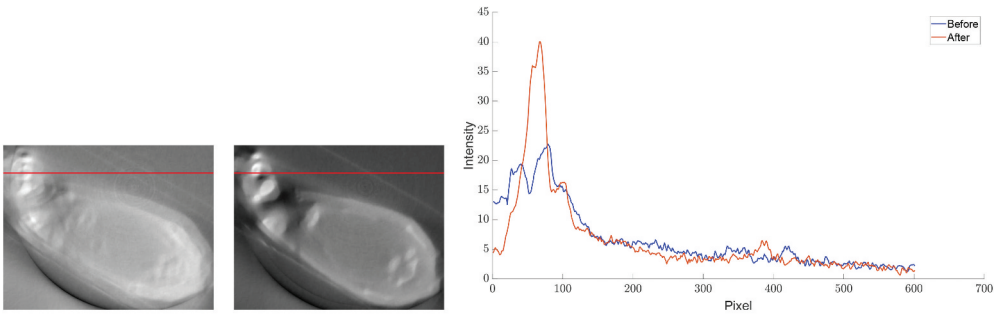

(a) before (b) after (c) intensity profile

Figure 5. Cross-sections from the reconstructed volumes of the piglet datasets. Using calibrated geometry for reconstruction, the bone structure of the piglet are clearly visible (b) compared to the reconstruction before correcting the geometry misalignment (a). The line profiles (c) show better contrast between the bone and the soft tissues after calibration (orange) compared to before correcting the geometry (blue).

Simulation experiments demonstrated the effectiveness of our proposed LEGO phantom to calibrate X-ray CT systems. It was shown that our proposed technique is able to distinguish between the geometry parameters of the detector and those of the object. Hence, the estimated detector geometry based on the scan of one object can be used to compensate for the geometry of a scan of another object acquired with the same system configuration. Misalignment artifacts were significantly suppressed in the CT reconstructed volumes after correcting the acquisition geometry of the $3D^2$YMOX system. Experiments with a real LEGO phantom and piglet datasets also demonstrated that our proposed method can be applied to practical X-ray CT systems. In conclusion, the proposed LEGO calibration procedure can be a valuable lab based solution to calibrate the geometry of X-ray CT systems.

In future work, we aim at extending the calibration procedure to a stereo cone beam geometry. Currently, one cone beam geometry is parameterized with 12 degrees of freedom. To fully characterize the configuration of the $3D^2$YMOX system more geometry parameters are required as it consists of a dual source/detector pair. Simultaneous, joint estimation of all 21 parameters is a future goal.

Acknowledgements

We would like to acknowledge Wim Huyge for the construction of the rotation stage of the $3D^2$YMOX system. This work has been supported by the University Research Fund, UAntwerp BOF-GOA 2016 33927, the Research Foundation - Flanders (FWO) SBO project MetroFlex (S004217N), and the European Commission through the INTERREG Vlaanderen Nederland program project Smart*Light (0386).

Disclosure statement

No potential conflict of interest was reported by the author(s).

Funding

This work was supported by the University Research Fund, UAntwerp BOF-GOA 2016 [33927]; EC INTERREG Vlaanderen-Nederland (Smart*Light) [0386]; Research Foundation – Flanders (FWO) SBO project MetroFlex [S004217N].

ORCID

J. De Beenhouwer http://orcid.org/0000-0001-5253-1274
J. Sijbers http://orcid.org/0000-0003-4225-2487

References

[1] Parkinson DY, Knoechelb C, Yang C, et al. Automatic alignment and reconstruction of images for soft x-ray tomography. J Struct Biol. 2012;177(2):259–266..
[2] Kingston A, Sakellariou A, Varslot T, et al. Automatic alignment and reconstruction of images for soft x-ray tomography. Med Phys. 2011;38(9):4934–4945.
[3] Jun K, Yoon S, Kwon K. Alignment solution for CT image reconstruction by fixed point and virtual rotation axis. Sci Rep. 2016;28(January). doi:10.1152/ajplegacy.1975.229.3.746
[4] Wang CC, Chiang CC, Liang B, et al. Fast projection matching for X-ray tomography. Sci Rep. 2017;7(1):1–11.
[5] Liu Y Improve Industrial Cone-Beam Computed Tomography by Integrating Prior Information [dissertation]. ETH Zurich; 2001.
[6] Cho Y, Moseley DJ, Siewerdsen JH, et al. Accurate technique for complete geometric calibration of cone-beam computed tomography systems. Med Phys. 2005;32 (4):968–983.
[7] Chetley Ford J, Zheng D, Williamson JF. Estimation of CT cone-beam geometry using a novel method insensitive to phantom fabrication inaccuracy: implications for isocenter localization accuracy. Med Phys. 2011;38(6Part 1):2829–2840.
[8] Mennessier C, Clackdoyle R, Noo F. Direct determination of geometric alignment parameters for cone-beam scanners. Phys Med Biol. 2009;54(6):1633–1660.

[9] Gross D, Heil U, Schulze R, et al. Auto calibration of a cone-beam-CT. Med Phys. 2012;39 (10):5959–5970.
[10] Quercioli F, Tiribilli B, Mannoni A, et al. Optomechanics with LEGO. Appl Opt. 1998;37 (16):3408.
[11] Levine Z, Grantham S. A low-cost fiducial reference phantom for computed tomography. J Res Natl Inst Stand Technol. 2008;113(6):335–340.
[12] 3D2YMOX; 3-Dimensional DYnamic MOrphology using X-rays; [cited on 2020 June 04]. Available from: https://www.uantwerpen.be/en/research-groups/3d2ymox/ (visited on 04/06/2020).
[13] Brainerd EL, Baier DB, Gatesy SM. et al. X-Ray reconstruction of moving morphology (XROMM): precision, accuracy and applications in comparative biomechanics research. J Exp Zool Part A Ecol Genetics Physiol. 2010;313 A(5):262–279.
[14] He K, Zhang X, Ren S, et al. Deep residual learning for image recognition. Proceedings of the IEEE Computer Society Conference on Computer Vision and Pattern Recognition Las Vegas, Nevada, United States; 2016. pp.770–778.
[15] Marinovszki A, De Beenhouwer J, Sijbers J An efficient CAD projector for X-ray projection based 3D inspection with the ASTRA Toolbox. 8th Conference on Industrial Computed Tomography, Wels, Austria; 2018.
[16] Vanderbei RJ, Shanno DF. An interior-point algorithm for nonconvex nonlinear programming. Comput Optim Appl. 1999;13(1573–2894):231–252.
[17] Ferrucci M Systematic approach to geometrical calibration of X-ray computed tomography instruments [dissertation]; 2018. Available from: https://lirias.kuleuven.be/retrieve/521553.
[18] Mahesh M. AAPM/RSNA physics tutorial for residents. Radio Graphics. 2004;24 (6):1747–1760.
[19] Sanctorum JG, Adriaens D, Dirckx JJJ, et al. Methods for characterization and optimisation of measuring performance of stereoscopic x-ray systems with image intensifiers. Meas SciTechnol. 2019;30(10):105701.
[20] Knorlein BJ, Baier DB, Gatesy SM, et al. Validation of XMALab software for Marker- based XROMM. J Exp Biol. 2016;219(23):3701–3711.
[21] Van Aarle W, Palenstijn WJ, Cant J, et al. Fast and flexible X-ray tomography using the ASTRA toolbox. Opt Express. 2016;24(22):25129–25147.
[22] Van Aarle W, Palenstijn WJ, De Beenhouwer J, et al. The ASTRA Toolbox: A plat- form for advanced algorithm development in electron tomography. Ultramicroscopy. 2015;157 (2015):35–47.
[23] Nguyen V, De Beenhouwer J, Sanctorum J, et al. A low-cost and easy-to-use phantom for cone-beam geometry calibration of a tomographic X-ray system. 9th Conference on Industrial Computed Tomography, (iCT 2019), Padova, Italy; 2019. pp. 1–8.